

RSC Advances



This is an *Accepted Manuscript*, which has been through the Royal Society of Chemistry peer review process and has been accepted for publication.

Accepted Manuscripts are published online shortly after acceptance, before technical editing, formatting and proof reading. Using this free service, authors can make their results available to the community, in citable form, before we publish the edited article. This *Accepted Manuscript* will be replaced by the edited, formatted and paginated article as soon as this is available.

You can find more information about *Accepted Manuscripts* in the [Information for Authors](#).

Please note that technical editing may introduce minor changes to the text and/or graphics, which may alter content. The journal's standard [Terms & Conditions](#) and the [Ethical guidelines](#) still apply. In no event shall the Royal Society of Chemistry be held responsible for any errors or omissions in this *Accepted Manuscript* or any consequences arising from the use of any information it contains.

Immune compatible cystine-functionalized superparamagnetic iron oxide nanoparticles as vascular contrast agents in ultrasonography

Sara Dolci¹, Valentina Domenici¹, Gianpaolo Vidili², Marco Orecchioni³, Pasquale Bandiera⁴, Roberto Madeddu⁴, Cristiano Farace⁴, Massimiliano Peana³, Maria Rosaria Tiné¹, Roberto Manetti², Francesco Sgarrella³ and Lucia Gemma Delogu^{*3}

¹ Department of Chemistry and Industrial Chemistry, University of Pisa, via Moruzzi 13, 56124 Pisa (Italy).

² Department of Clinical and Experimental Medicine, University of Sassari, Viale San Pietro 07100 Sassari, Italy.

³ Department of Chemistry and Pharmacy, University of Sassari, via Muroni 23, 07100 Sassari, Italy.

⁴ Department of Biomedical Sciences, University of Sassari, Viale San Pietro 43c, 07100 Sassari, Italy.

* Corresponding author: Lucia Gemma Delogu, E-mail: lgdelogu@uniss.it

Abstract

Superparamagnetic iron oxide nanoparticles (SPIONs) have been extensively investigated for many biomedical applications. A good quality functionalization that combines imaging goals with a high-level biocompatibility remains one of the challenges for particle translation into medical practice. Here, we focus on a new functionalization of SPIONs with cystine (Cy-SPIONs). Cystine is able to make SPIONs stable and dispersible in water and in culture cell media. New insights are provided into the biological and immune effects of Cy-SPIONs with a wide variety of standard and molecular assays to evaluate cytotoxicity, cell activation, cytokine release and the expression of 84 genes related to immune responses.

A good immune biocompatibility of Cy-SPIONs on primary immune cells was found. The great potential of Cy-SPIONs for further *in vivo* studies and as contrast agents for magnetic resonance imaging (MRI) is highlighted. In addition, we also exploited ultrasonography, since it is a safer, less expensive and common imaging technology. The good echogenic properties of Cy-SPIONs in water and in whole blood are shown, both *in vitro* and in a phantom vein for bloodstream simulations.

Our results open up a new scenario for future applications of cystine-functionalized SPIONs as immune-compatible ultrasound and MRI contrast agents.

Keywords: Superparamagnetic iron oxide nanoparticles, immune system, MRI, ultrasounds, gene expression, cytokines

Footnotes

Electronic Supplementary Information (ESI) available: TEM images of PBMCs Cy-SPIONs treated and Heat Map description table.

Introduction

Magnetic nanoparticles have attracted much interest among scientists and the general public ¹ as advanced nanomaterials for several types of applications, as well as for drug and gene delivery or/and imaging agents ^{2, 3}. Superparamagnetic iron oxide nanoparticles (SPIONs) have been investigated for biomedical applications such as tissue repair, immunoassays, detoxification of biological fluids, hyperthermia, drug delivery, probes, in vitro cell separation and to produce antibiotic-resistant biofilms. They are thus them important candidate materials for new perspectives in nanomedicine ⁴.

Since 2005 SPIONs were introduced as tracers for tomographic magnetic particle imaging modality ⁵. One of the major aims of scientists in improving diagnostic technologies is to create better contrast agents and superior imaging systems, however every system has its weaknesses ⁶.

SPIONs are excellent materials for multimodal imaging ⁷. One interesting modality is the use of MRI and ultrasonography (US) at the same time. US is fundamental in everyday clinical practice and many researchers are now using new nanomaterials to improve this imaging methodology which is very economical and safe ⁸⁻¹⁰. Further innovations in the development of diagnostic tools that possess the advantages of MRI and US dual-modality properties are still needed, i.e. the US-triggered release of therapeutic agents to tumor cells for the battle against cancer ¹¹⁻¹³.

In order to achieve efficient imaging applications and loading capacity of SPIONs, one of the main challenges is to obtain nanoparticles with good hydrophilic surface coating ^{14-15, 16}. To achieve this goal the functionalization is of fundamental importance for the good biocompatibility and safety of SPIONs. Thus, the first concern is to reduce both SPIONs' instability in biological media and the concentration necessary for efficient functionalization. At the same time this would minimize toxic effects and costs, while maintaining a high-resolution contrast. In a previous work, we reported a new method to increase the stability of SPIONs in biological media through the surface coating of SPIONs with cystine ¹⁷. Cystine acts as a precursor for proteins, antioxidant glutathione (GSH) biosynthesis, as well as maintaining physiological redox conditions inside/outside the cell ¹⁸. We found that this new type of functionalization improved SPIONs' hydrophilicity and water stability ^{17, 19}. Preliminary NMR relaxation studies have also highlighted their interesting properties as Magnetic Resonance Imaging (MRI) contrast agents. However, an extensive and molecular assessment of the potential impact of SPIONs on immune cells is still lacking. Toxicity and immune compatibility are still major blocks to the use of nanomaterials in medicine ²⁰⁻²⁴. Thus, all the applications cited above normally require intravenous administration and the first cells that come

in contact with foreign substances are blood immune cells. It is therefore necessary to analyze the possible impact of SPIONs on immune cells also using a molecular approach such as gene expression analysis. Jin R *et al.*¹⁵ highlighted the importance of immunological studies especially for the potential use of SPIONs in future pre-clinical testing, considering also that any difference in nanoparticle-conjugated moiety can lead to a different toxicological and immune impact. SPIONs have been used for MRI imaging of inflammation sites in the body, mainly looking at the monocytes/macrophage interaction and at the inflammation response in tissue^{25,26}.

Most studies that have analyzed the effect of SPIONs on immune cells, have only considered one type of immune cell population, such as monocytes or macrophages²⁷⁻³¹. Instead in this study we used total PBMCs for our analysis, which include many different cell populations, such as T cells, B cells, monocytes, NK cells and dendritic cells.

Our approach better simulates the normal bloodstream behavior with the interaction of different types of cells that can modulate each other's activations against foreign substances, such as nanoparticles. The *ex vivo* analysis also gives a better overview of the real action of Cy-SPIONs on immune cells, opening up the way for future pre-clinical application studies. To lay the foundation of our cystine functionalized SPIONs (Cy-SPIONs) in imaging, it is also critical to assess their contrast properties. We thus decided to start from the safest imaging modality: ultrasonography.

In this paper we focus on Cy-SPIONs, which are easily dispersible in biological media. We provide new insights into the biological and immune effects of Cy-SPIONs with a standard and molecular range of assays to evaluate the cytotoxicity (*ex vivo* and *in silico* in a synthetic microvasculature network chip after US), cell activation, cytokine release and the expression of 84 genes related to the immune response. In addition, the echogenic properties of Cy-SPIONs were assessed *in vitro* in degassed water and *ex vivo* in human blood. We show how Cy-SPIONs could be used in US as safety novel intravenous contrast agents.

Experimental section

Materials

Iron pentacarbonyl ($\text{Fe}(\text{CO})_5$), oleic acid ($\text{C}_{18}\text{H}_{34}\text{O}_2$), dioctyl ether ($\text{C}_{16}\text{H}_{34}\text{O}$), trimethylamine N-oxide ($\text{C}_3\text{H}_9\text{NO}$), ethanol, L-cysteine ($\text{C}_3\text{H}_7\text{NO}_2\text{S}$) and hexane were purchased from Sigma-Aldrich®. Toluene was distilled from the usual drying agents under nitrogen. All reactions were carried out

under a nitrogen atmosphere using standard Schlenk techniques. The reaction vessels were oven-dried at 130°C prior to use, evacuated (10⁻² mmHg) and then filled with nitrogen.

Synthesis and characterization of Cy-SPIO nanoparticles

To obtain monodisperse, highly crystalline and nanometer-size iron oxide nanoparticles, oleate-coated SPIONs (OA-SPIONs) were prepared by following a thermal decomposition method³² and then functionalized with cystine using a ligand exchange reaction, as described in ref. [24]. Fe(CO)₅ (0,66 mL, 5 mmol) was added to a solution of oleic acid (1.59 mL, 5 mmol) in dioctyl ether (50 mL) at 373 K, under nitrogen atmosphere. The mixture was heated to reflux (559 K) for 1 hour. After cooling to room temperature, anhydrous trimethylamine N-oxide (376 mg, 5 mmol) was added and the mixture heated again (to 413 K for 2 h and then to reflux for 1 h). Ethanol was used to precipitate the resultant OA-SPIONs, which were separated by centrifugation and dried *in vacuo* (1.0 × 10⁻³ Torr).

Cystine coated SPIONs (Cy-SPION) were prepared by dissolving OA-SPIONs (506.4 mg, iron content 30.3% (w/w)) in 80 mL of toluene and adding an excess of L-cysteine (1.485 g, 12.25 mmol) under nitrogen atmosphere. The resulting brown mixture was heated to reflux (383 K) for about 4 h, up to the precipitation of a brown solid to the bottom of the flask that produced a colorless solution. The solid was washed with hexane, collected by centrifugation and dried *in vacuo* (1.0 × 10⁻³ Torr). The solid was then washed with water to remove the free L-cysteine and dried with a vacuum pump. During the exchange reaction, the oxidation of cysteine to cystine takes place, promoted by Fe₂O₃¹⁷, until complete replacement of the oleic acid by the *in situ* generated cystine.

The iron content of SPIONs was determined by the spectrophotometric method^{17, 19}. The SPION size and morphology were determined by analyzing TEM images obtained with a Philips CM 12 operating at 100 kV. Samples were prepared by placing one drop of a solution of Cy-SPION in water on the specimen grid and allowing the solvent to evaporate. The SPION dimensions were analysed with ImageJ. The surface functionalization of Cy-SPIONs was characterized by several complementary techniques^{17, 19}.

MRI phantom analysis of Cy-SPION dispersions

Additional experiments were carried out to investigate the stability of water Cy-SPION dispersions and their MRI potentialities. In particular, *in vitro* ¹H NMR relaxation rates measurements were

performed on aqueous Cy-SPION dispersions containing increasing iron concentrations using the 7 Tesla 950-MR scanner GE Healthcare machine.

Approximately 13 mg of Cy-SPIONs were introduced in a vial and 1mL of deionized water were added. After 10 minutes of sonication with a BRANSONIC 220 water bath sonicator, the vial was centrifuged for 5 minutes at 3500 rpm to remove nanoparticles in the mixture. The solution was then diluted in various ratios in order to obtain Cy-SPION aqueous dispersions at various concentrations. NMR glass tubes containing Cy-SPION dispersions with [Fe] equal to 0.320, 0.213, 0.160 and 0.106 mM were placed in an agar phantom and the proton NMR relaxation times, T_1 and T_2^* , were recorded using standard inversion recovery (IR) and spin echo (SE) sequences, respectively.

Ultrasound Imaging

Technos MPX (Esoate) was used for all ultrasonography experiments. The analyses were recorded at 14-MHz; the instrument was set in conventional US modality (B mode), depth 31 mm, gain 170, -1.3 dB, and mechanical index=1. The US signal was calculated using Adobe Photoshop CS5 (Adobe Systems). US signal is reported in 8-bit gray scale intensity from 0 to 255 shades of gray. For US images on degassed water, the areas of interest were selected. A comparison of samples was performed on the same areas with 29205 analyzed pixels. Experiments were done in triplicate.

Cell culture maintenance

Jurkat cells (T cell line) and peripheral blood mononuclear cells (PBMCs) were cultured in RPMI 1640 medium containing 1% antibiotic-antimycotic mixture and 10% heat-inactivated fetal bovine serum (FBS) (Invitrogen) in an incubator at 37 °C in a 5 % CO₂. Human PBMCs were obtained from blood samples from healthy male donors (25-50 years old) using a standard Ficoll-Paque (GE Healthcare) separation. All the donors provided written informed consent. The study was reviewed and approved by the ethics committee of the University of Sassari (Italy).

Cy-SPION viability and activation on immune cells

For the viability assay, PBMCs were transferred to a 24-well plate and treated for 24 h in triplicate with 50, 100, 200 $\mu\text{g mL}^{-1}$ of Cy-SPION or left untreated. Cells were treated with EtOH 70% as a positive control and then washed in cold PBS before the staining reaction. After incubation, cells

were harvested, washed in cold PBS and re-suspended in 1mL of PBS at 1×10^6 cells mL^{-1} . Viability was assessed by the LIVE/DEAD[®] Fixable Dead Cell Stain Kit (Invitrogen), which uses an amine-reactive fluorescent dye, cells with compromised membranes (late apoptotic and necrotic). The dye reacts with free amines both inside the cell and on the cell surface, yielding intense fluorescent staining. In viable cells, the dye reactivity is restricted to the cell surface amines, resulting in less intense fluorescence.

To detect cells undergoing apoptosis and necrosis, Annexin-V FITC and propidium iodide staining were used (Invitrogen). Cells were analysed by flow cytometry (FACS Calibur BD-Bioscience). To identify T cells and specifically CD8+ and CD4+ T cell populations, the populations were isolated using specific antibodies: CD3 for the entire T cell gating, CD8 and CD4 for Cytotoxic T cells and T helper cells, respectively. To assess the cell activation, specific antibodies were used against CD25, CD69 and CD30 cell activation markers. All the antibodies used were purchased from BD Biosciences. Data analysis was performed by flow cytometry (FACS Calibur, BD Biosciences) using CellQuest[®] software (BD Biosciences).

Proliferation assay

To perform the proliferation assay, the Click-iT EdU Alexa Fluor 488 Flow Cytometry Assay Kit (Life Technologies) was used. The experiments were performed according to the manufacturer's instructions. Cells were seeded at the concentration of 1×10^6 cells mL^{-1} in 96 multi-well rounded bottom plates. PBMCs were treated with Cy-SPIONs (50, 100, 200 $\mu\text{g mL}^{-1}$) and phytohemagglutinin 2% (PHA) and interleukin 2 (IL2) 30 u/mL or left untreated. 5-ethynyl-2-deoxyuridine (EdU) was added in sterile conditions 16 h before the analysis. After 72 h of incubation, cells were harvested, washed in PBS, fixed with 4% paraformaldehyde, washed in PBS + 1% BSA, permeabilized with a saponin-based reagent, and prepared for the Cu-assisted EdU-Azide Click-iT reaction. The reaction occurs after adding 500 μl of Click-iT reaction cocktail (PBS, CuSO_4 , fluorescent dye azide and reaction buffer additive) to each sample. Analyses were performed by flow cytometry (FACS Calibur BD Bioscience) using CellQuest[®] software (BD Biosciences). A total of 50,000–100,000 events were recorded.

Idealized synthetic microvascular network (SMN) and related viability test

The Synthetic Microvascular Networks or SMNs were purchased from SYN VIVO CFDRS Huntsville, Alabama, USA. The SMN is able to perfectly reproduce a trait of the rat microvasculature (vessels

depth of 100 μm). The chip was developed using a standard photolithography process³³. The SMN was used in order to assess the potential impact of Cy-SPIONs on human primary immune cells in an *in vivo* like simulation under ultrasonography. Tygon tubing was inserted into the inlet/outlet ports of the device, a syringe was loaded onto a syringe pump and PBMCs with or without Cy-SPIONs (200 $\mu\text{g}/\text{mL}$) injected at rates flow of less than 1 $\mu\text{l}/\text{min}$. After 24 h of incubation at 37° in 5% of CO_2 , the device was covered with plastic paper and gel for ultrasonography, and sonication with an US probe was then performed for 10 minutes. PBMCs with or without Cy-SPIONs were immediately extracted and cell count performed with a trypan blue solution (4%, Sigma Aldrich) under inverted microscopy (Nikon Instruments Inc.).

Immune cell gene expression analysis

Total RNA was extracted from Jurkat cells after incubation with SPIONs 200 $\mu\text{g mL}^{-1}$. RNA purification was performed with TriZol Reagent (TriZol, Invitrogen, Carlsbad, CA, USA). After extraction, cDNA synthesis was performed using a SuperScript® II reverse transcriptase (Invitrogen) following the manufacturer's instruction. Comparison of the relative expression levels of 84 immune response genes was performed with a RT2 Profiler PCR Array (PAHS-052ZD, Superarray Bioscience Corporation, Frederick, MD), (instrument CFX96 Bio-Rad). Data were analyzed by the comparative threshold cycle (CT) method. The relative quantification of the gene expression using the $2^{-\Delta\Delta\text{Ct}}$ method correlated with the absolute gene quantification obtained using a standard curve. Data were analyzed with RT2 profiler PCR array data analysis software (<http://www.superarray.com/pcrarraydataanalysis.php>). Untreated cells were compared to Cy-SPIONs treated samples. Experiments were performed in triplicate.

Results and Discussion

Synthesis and characterization of Cy-SPIONs

In this work we studied the bio-immune impact and properties in ultrasound imaging of SPIONs with a new type of functionalization, using cystine. Cystine has a fundamental biological role as a component of antioxidant glutathione (GSH), and also for the maintenance of physiological redox conditions inside and outside the cell. The cystine receptor is also present in many cells of the body and is responsible for many biological processes¹⁸.

Our previous studies^{17, 19} showed that Cy-SPIONs are stable nanoparticles and very interesting for medical applications, since their dispersion in water is quite stable. The preparation of Cy-SPIONs involves the synthesis of oleate-coated SPIONs (OA-SPION) by a thermal decomposition method³⁴ and the subsequent functionalization by a ligand exchange reaction with L-cysteine.

Using X-ray diffraction, magnetic properties and microscopy analysis (i.e. TEM and AFM), it was possible to characterize the chemical structure of both the magnetic core and the surface coating of Cy-NPs, as previously reported¹⁹. In particular, the ligand exchange between oleate and cysteine was fully clarified, showing that the complete oxidation of cysteine to cystine produced an external cystine-shell, which is fundamental for biomedical applications. The water stability of Cy-NP dispersion is very important and the water dispersion was confirmed to be stable for more than 7-8 h¹⁹. Concerning the chemical-physical properties of these Cy-NPs, both spectroscopic (FT-IR) and microscopy (AFM and TEM) studies agree with the schematic picture reported in **Fig. 1A**. The average iron oxide core dimension of Cy-SPIONs ranges from 3.6 and 3.95 nm, as determined independently by three methods (namely AFM, TEM and magnetic curve analysis¹⁷).

As an example, a TEM image of Cy-SPIONs is shown in **Fig. 1B** and the corresponding dimension distribution is reported in **Fig. 1C**. According to the analyses of five new TEM images obtained as reported in the previous section, the average diameter of these nanoparticles was 3.95 nm (with a standard deviation of 0.41 nm), in agreement with previous investigations^{17, 19}.

In our previous work¹⁷, a preliminary study of the ¹H NMR relaxation properties at low and high magnetic fields indicated the potential of Cy-SPION water dispersions as MRI contrast agents. At concentrations lower than 0.5mM, we found that the spin-lattice relaxation rate R_1 ($=1/T_1$) decreases by increasing the value of the field, while the spin-spin relaxation rate R_2 ($=1/T_2$) has the opposite trend. This is interesting for MRI applications, since the efficiency of contrast agents for imaging applications is related to the ratio R_2/R_1 .

The possibility of changing this ratio by changing the magnetic field strength opens new possibilities of using our Cy-SPIONs as negative as well as positive contrast agents. To confirm such behavior¹⁷, we report new data acquired at 7 Tesla (corresponding to a ¹H Larmor frequency of

300 MHz) by an MRI machine. By using a phantom, prepared as described in the previous section, we collected several MRI images and calculated the relaxation rates, R_1 and R_2 , of four Cy-NP dispersions with different iron concentrations (indicated in **Fig. 2** as “region of interest”, namely ROI) and one sample of pure water (ROI number 5), as a reference.

The enhancement contrast ratio (EHC) was calculated by using the following equation, in order to evaluate the contrast power:

$$EHC(\%) = \left(\frac{(SI_{Cy-NP} - SI_{water})}{SI_{water}} \right) \times 100$$

where SI_{Cy-NP} and SI_{water} correspond to the signal intensity evaluated on the MRI image for the Cy-SPION dispersions and water reference, respectively. EHC, R_1 and R_2 of the Cy-SPIONs water dispersions are reported in **Fig. 2A**, while a MRI T_2 -weighted image is shown in **Fig. 2B**.

From this investigation we can confirm that Cy-SPIONs are stable in water. In addition, the values of EHC and the fact that the ratio R_2/R_1 is in the range 20-50 for concentrations of Cy-SPIONs in the range 0.106-0.320 mM, indicate that these nanoparticles act as negative MRI contrast agents.

In the following sections, these nanoparticles are investigated in order to check, first, their biocompatibility and, second, their possible use as ultrasound contrast agents.

Cy-SPION potential in ultrasonography imaging

The classical application of SPIONs is as contrast agents in MRI. The recent interest in multimodal imaging has thus opened up new perspectives, indeed each imaging technique has advantages but also intrinsic limitations, in some cases low sensitivity, in others low spatial resolutions³⁵. Many groups have reported the use of SPIONs encapsulated into other particles such as microbubbles, vesicles or liposome for a bimodal imaging using MRI and US³⁶⁻⁴⁰. Microbubbles are the most commonly used US contrast agents for medical applications, thanks to their highly echogenic *in vivo* properties⁴¹. The presence of SPIO nanoparticles in the bubble shell can alter the surface tension of bubbles, boosting the acoustic impedance and enhancing the detectable backscatter. Yang F *et al.*, for example, used SPIONs conjugated microbubbles improving their capabilities in US imaging and also, thanks to SPIONs, producing a good MRI contrast³⁷.

The size of the most common microbubble-based US contrast agent (1–8 μm) renders them as merely intravascular flow tracers and the SPIONs encapsulated in microbubbles or vesicles reached these dimensions. In contrast, the chemico-physical characteristics of SPIONs (i.e., 4 nm in diameter in the present study) make them potentially capable of extravasating and reaching a

tumor region, which can exhibit a vascular pore size up to 780 nm⁴². The small size of SPIONs means that they can cross endothelial barriers and, as targetable materials, can reach a tumor region, acting at the same time as vehicles for therapeutic agents³².

To the best of our knowledge few studies have tested the US ability of SPIONs without any coating. For example, Mehrmohammadi M. *et al.* successfully used SPION (Feridex) for magneto-motive US imaging. However, they did not find a significant US signal from the free SPIONs in a tissue phantom, and they stated that SPIONs are not useful US contrast agents due to their weak reflectivity⁴³. We are aware of the fact that the modification of SPIONs with other molecules or particles may change their contrast properties⁴⁰.

In order to investigate our uncoated Cy-SPIONs as potential ultrasound contrast agents, after having assessed the uptake and ruled out the possible cytotoxic of our nanoparticles at different concentrations, we assessed the echogenic property of Cy-SPIONs in dose responses at 50, 100 and 200 $\mu\text{g mL}^{-1}$ in degassed water. To avoid the possible bubble-formation after injection of Cy-SPION solution we carefully suspend the Cy-SPIONs in degassed water for all the experiments. **Fig. 3A** shows visible and well-dispersed nanoparticles under ultrasonography. The white area visible in the US image suggests the high echogenicity of Cy-SPIONs. Interestingly, the US signal of dispersed Cy-SPIONs was three times more intense than same degassed plain water used as a negative control (11.0 vs. 43.0, respectively; $P < 0.05$) (**Fig. 3B**).

In view of the results obtained from the experiments in water, we tested the echogenic propriety of Cy-SPIONs on whole blood. Intriguingly, the red arrows in the US image (**Fig. 3C**) indicate a visible and strong US signal of Cy-SPION nanoparticles well dispersed in whole blood.

To confirm these data, we performed an experiment with a phantom vein and human blood to simulate the bloodstream conditions (**Fig. 3D**). The brightness of Cy-SPIONs after injection in the phantom vein under ultrasonography was detected (**Fig. 3D**). These experiments proved that Cy-SPIONs were also perfectly visible in a complex fluid such as blood that *per se* has a high background signal compared to water. Our data are not in agreement with the weak reflectivity of SPIONs found by Mehrmohammadi M. *et al.* The higher US signal that we found with our uncoated Cy-SPIONs could be due to the different functionalization compared to Feridex used by Mehrmohammadi M *et al*⁴³. Thanks to the high dispersibility in water of our CY-SPIONs, they are able to give a strong US signal.

Uptake and biocompatibility of Cy-SPIONs

SPIONs uptake has already been reported for different cell lines⁴⁴. Here for the first time we assessed their ability to cross the membrane as cystine functionalized SPIONs in *ex vivo* human PBMCs from healthy donors (**S. Fig. 1**). Cells were incubated for 24 h with Cy-SPIONs at high doses ($200 \mu\text{g mL}^{-1}$) and analyzed by TEM. **S. Fig. 1(A)** shows a representative image of the control samples, where all organelles are clearly visible and correspond to the normal functionality of cells. **S. Fig. 1(B)** shows the presence of a large number of Cy-SPION inside the cells in the treated samples. Due to their phagocytic properties, monocytes were the cell population with the highest capacity of uptake (>70% of visible Cy-SPION clusters) compared to the other cell types present in PBMC populations (T cells, B cells, natural killers).

Some toxicology studies with SPIONs lacking in bio-functionalization have highlighted the possible toxicity of these nanoparticles^{45,46}.

To check the cell compatibility of Cy-SPIONs, we performed multiparametric flow cytometry assays looking at early and late apoptosis, necrosis, cell membrane status and proliferation on *ex vivo* immune cells (**Fig. 4**). First, we performed a live/dead staining and apoptosis and necrosis assay in dose response ($50, 100, 200 \mu\text{g mL}^{-1}$ of Cy-SPIONs) on cells incubated for 24 h (**Fig. 4A and 4B**). Ethanol incubation was used as a positive control. We chose these concentrations following the work of Naqvi S *et al*, where the authors studied the effect of SPION concentration (from 25 to $500 \mu\text{g mL}^{-1}$) on immune cells, specifically on macrophages⁴⁷. Even at high concentrations of $200 \mu\text{g mL}^{-1}$, Cy-SPIONs did not exert any toxicity.

Data in agreement with Yeh CH *et al*; the authors pointed out that the Resovist (FDA approved) do not give any toxicity in macrophage also at the higher concentration used ($200\mu\text{g/mL}$)⁴⁸. Recent studies also displayed that there was no toxicity in murine macrophages after overnight labeling with Ferumoxides (Feridex, Advanced Magnetics, USA, Endorems, Guerbet, France; dextran-coated, hydrodynamic diameter of 120–180 nm)⁴⁹.

Differences from the control percentage were not statistically significant, including annexin-V staining (as shown in **Fig. 4A and 4B**). In addition, we assessed whether Cy-SPIONs impact cellular proliferation (**Fig. 4C**) of total PBMCs and through the specific gating of T cells CD4+ and CD8+. We focused on the T cell subpopulation since it is the most abundant on PBMCs (up to 40%) and is the easiest one to culture *ex vivo* for a long time, as required for proliferation assays.

Samples were treated with phytohemagglutinin at 2% and $30 \mu\text{g/mL}$ of interleukin 2 for three days to boost the proliferation in the presence of magnetic particles. Control samples were left untreated. A staining with 5-ethynyl-2'-deoxyuridine (Edu) Alexa-Fluor conjugated was performed,

and Edu was incorporated into DNA during active DNA synthesis. No significant difference in treated samples compared to controls was observed. However, at $200 \mu\text{g mL}^{-1}$ we found a decrease in proliferation for each cell population.

These results confirmed the lack of cytotoxicity of Cy-SPIONs. The bio-immune-compatibility of Cy-SPIONs found may be related to the physiological functions of cystine as a component of glutathione and therefore as protection for the cells from oxidation stress.

Biocompatibility of Cy-SPION under US into idealized synthetic microvascular network (SMN).

Additional biocompatibility experiments were performed using a microfluidic device (SynVivo technology), which simulates the micro-vascular system of mice (**Fig. 5**). We used purified PBMCs treated with the higher concentration ($200 \mu\text{g mL}^{-1}$) of Cy-SPIONs; untreated PBMCs were used as a control. The cells were added to the microfluidic device and after 24 h of incubation with Cy-SPIONs were exposed to US for 15 minutes (the time necessary for US exams on humans) on top of the microfluidic channel, and then a viability assay with a Trypan Blue exclusion test was performed (**Fig. 5A**). Red arrows highlighted well-dispersed Cy-SPIONs inside the microchannel (**Fig. 5B**). No statistically significant difference in terms of percentage of dead cells between treated and control samples was found (**Fig. 5C**). We assume that our Cy-SPIONs are perfectly biocompatible also under US, improving their future application in *in vivo* applications.

Cy-SPION impact in human PBMCs

The preservation of normal immune functions is fundamental in the use of Cy-SPIONs for potential treatment or the future diagnosis of any disease. The analysis of activation reveals the functionality of immune cells. We thus investigated the expression of the activation-related surface molecules: i) CD69, a member of the C-type lectin superfamily (Leu-23), one of the earliest cell surface antigens expressed by immune cells following activation; ii) CD25 (alpha chain of the IL-2 receptor), a late activation antigen; and iii) CD30, a cell membrane protein of the tumor necrosis factor receptor family. Due to their well-known activation properties, concanavalin A (Con A) and lipopolysaccharide (LPS), were used as a positive control. **Fig. 6A** shows the percentage of CD25+ cells after incubation with different concentrations of Cy-SPIONs, highlighting the total comparability of treated samples with controls. We also found (**Fig. 6A**) the same results for the CD69 and CD30 expression markers. The total absence of activation after particle incubation is also reported. As stated by Mahmoudi M *et al.* there is little direct evidence on the induction of

inflammatory pathways and cytokines by engineered SPIONs (both uncoated and coated) *in vivo* and *in vitro* ⁴⁵.

To fill this gap in the literature we studied the secretion of a wide variety of cytokines after incubation with 200 $\mu\text{g mL}^{-1}$ Cy-SPIONs in cells. In our analysis we examined four primary cytokines: TNF α , IL10, IL6 and IL1 β (**Fig. 6B**) as they are among the most important cytokines secreted from PBMCs. Multiplex ELISA assay was used for the detection.

Interestingly, we found a Cy-SPION dose-dependent increase of TNF α , IL10 and IL6 (p-value < 0.05). The cytokines found expressed such as IL6 and TNF α are normally secreted by monocytes/macrophages and their action is normally directed on the activation of the acute inflammation process ⁵⁰. IL10 is a cytokine mainly secreted by activated macrophages that through a negative feedback directly control and decrease the immune response ⁵¹. This action, as previously proved by many research groups ⁵²⁻⁵⁵, could be the possible consequence of the uptake of Cy-SPIONs by monocytes shown in **S. Fig. 1**.

Thus, studies conducted *in vitro* on the effect of SPIONs on macrophage functions have revealed modifications in cellular behaviors as well as in the modulated cytokine expressions ^{56, 57}. For instance, Hsiao JK *et al.* studied the response of clinically-used SPION ferucarbotran (Resovist) loading upon macrophage and found that high doses of SPIONs induced the secretion of TNF- α and resulted in cellular activation through the production of nitric oxide ⁵⁷. Also in the study of Yeh CH *et al.* the cytokine secretion analysis indicated that Resovist could elicit the production of pro-inflammatory cytokines such as TNF- α , IL-1 β and IL-6, but their levels were much lower than those with lipopolysaccharide (LPS) stimulation ⁴⁸. We found similar results with our Cy-SPION compared to other already approved SPIONs for MRI imaging evidencing no significant toxicity on immune cells ^{58, 59}.

The uptake of SPIONs by phagocytic monocytes and macrophages provides a valuable *in-vivo* tool by which imaging techniques can be used to monitor the involvement of macrophages in inflammatory processes such as multiple sclerosis, traumatic nerve injury, stroke, brain tumors, and vulnerable plaques in carotid artery.

Our data are in accordance with findings on commercial clinically approved SPIONs to be used as SPION-based MRI contrast agents such as Resovist, Feridex and Combidex, which are coated with dextran, other carbohydrates or citrate-stabilized particles. SPIONs with other functionalizations (polymers, metals, silica) are in the development phase ⁵².

To better understand all aspects of Cy-SPIONs interaction with immune cells, an extensive genome

study with an RT2 Profiler PCR Array testing was performed, studying the expression of 84 key genes on immune responses (**Fig. 7**). For a clear picture of gene expression, we focused on a well established T cell line (Jurkat) for two critical reasons: i) it is a good model particularly for the adaptive the immune-cell response; ii) T cells are the most abundant population in the blood flow, therefore their reactions can give a wide picture on SPIONs impact.

The heatmap (**Fig. 7A**) shows 84 genes displayed for fold change variations in comparison to the medium control and colored by their standardized expression value (red= high expression; green= low expression). The induction of TNF expression found was in perfect agreement with the cytokine data. The other genes modulated with a fold change higher than 2 were: B2M, MAPK1, TLR2, IRAK1, TYK2, NLRP3 and HLA-A (**S. Fig. 2**). The up-regulation of the toll-like receptor 2 (TLR2) in T cells led us to hypothesize that Cy-SPIONs come in contact with immune cells through a toll-like receptor. This interaction may also be responsible for the up-regulation of genes such as MAPK1, TYK2 and IRAK1, which are normally implicated in signal transduction. MAPK/ERK pathways are responsible for many functions such as cell growth and proliferations. TYK2 and IRAK1 also encode for kinases that are responsible for interferon and IL1 secretion. These data were confirmed in the Scatter Plot (**Fig. 7B**); all genes were shown in accordance to fold regulation. Only two, NLRP3 and HLA-A, were up-regulated with a fold regulation greater than 4. **Fig. 7C** reports the up-regulated genes. The modulated genes found are not implicated with a significant modification in cell functionality, indeed the few genes up-regulated and also the activation markers analysis did not show any cell-activation response.

Conclusions

To conclude, in this work we give new insight into the use of cystine functionalized SPIONs in imaging, not only for MRI but also for ultrasonography due to their echogenic properties in water and blood, as shown in the present study. Intriguingly the small size of our Cy-SPIONs make them able to cross endothelial barriers and, as targetable materials, to potentially reach a tumor region, acting at the same time as vehicles for therapeutic agents. The potentiality of our Cy-SPIONs to extravasate and localize in a tumoral region highlight that Cy-SPIONs could be successfully exploited for theranostic applications. Moreover our data clearly point out the good immune and biocompatibility of Cy-SPION, with absence of activation stimuli on treated PBMCs.

These findings make Cy-SPIONs perfect materials for new in vivo dual mode imaging studies where

the preferential route of administration is by intravenous injections.

Acknowledgments

We thank the staff of CFD Research Corporation (Huntsville, Alabama, USA) for their technical help. The authors would also like to thank Prof. Maja Remskar for the TEM images, and Dr. Michela Tosetti for giving us access to the IMAGO 7 Foundation equipment for MRI preliminary investigations. V. Domenici and M.R. Tinè thank MIUR for the project entitled “Nanoscale functional organization of (bio)molecules and hybrids for targeted application in sensing, medicine and biotechnology”, PRIN 2010-2011, No. 2010C4R8M8. This work was also partly supported by the Fondazione Banco di Sardegna (grant N° 2013.1308, 2014.6035 to L.G.D.), the Sardinia Region (grant N° CRP-59720 to L.G.D.) and the Gianfranco del Prete Association “The future: medicine, biology and nanotechnology Award” to L.G.D.

Reference

1. G. Sechi, D. Bedognetti, F. Sgarrella, L. Van Eperen, F. M. Marincola, A. Bianco and L. G. Delogu, *Nanomedicine*, 2014, **9**, 1475-1486.
2. C. Wu, F. Gong, P. Pang, M. Shen, K. Zhu, D. Cheng, Z. Liu and H. Shan, *PloS one*, 2013, **8**, e66416.
3. P. Pang, C. Wu, M. Shen, F. Gong, K. Zhu, Z. Jiang, S. Guan, H. Shan and X. Shuai, *PloS one*, 2013, **8**, e76612.
4. A. K. Gupta and M. Gupta, *Biomaterials*, 2005, **26**, 3995-4021.
5. B. Gleich and J. Weizenecker, *Nature*, 2005, **435**, 1214-1217.
6. S. Lee and X. Chen, *Molecular imaging*, 2009, **8**, 87-100.
7. F. Liu, S. Laurent, H. Fattahi, L. Vander Elst and R. N. Muller, *Nanomedicine*, 2011, **6**, 519-528.
8. S. G. Zheng, H. X. Xu and H. R. Chen, *World journal of radiology*, 2013, **5**, 468-471.
9. M. Postema and O. H. Gilja, *World journal of gastroenterology : WJG*, 2011, **17**, 28-41.
10. L. G. Delogu, G. Vidili, E. Venturelli, C. Menard-Moyon, M. A. Zoroddu, G. Pilo, P. Nicolussi, C. Ligios, D. Bedognetti, F. Sgarrella, R. Manetti and A. Bianco, *Proceedings of the National Academy of Sciences of the United States of America*, 2012, **109**, 16612-16617.
11. F. M. Kievit, Z. R. Stephen, O. Veiseh, H. Arami, T. Wang, V. P. Lai, J. O. Park, R. G. Ellenbogen, M. L. Disis and M. Zhang, *ACS nano*, 2012, **6**, 2591-2601.
12. Y. Song, Z. Huang, J. Xu, D. Ren, Y. Wang, X. Zheng, Y. Shen, L. Wang, H. Gao, J. Hou, Z. Pang, J. Qian and J. Ge, *Biomaterials*, 2014, **35**, 2961-2970.
13. M. K. Yu, D. Kim, I. H. Lee, J. S. So, Y. Y. Jeong and S. Jon, *Small*, 2011, **7**, 2241-2249.

14. B. Basly, G. Popa, S. Fleutot, B. P. Pichon, A. Garofalo, C. Ghobril, C. Billotey, A. Bernard, P. Bonazza, H. Martinez, D. Felder-Flesch and S. Begin-Colin, *Dalton transactions*, 2013, **42**, 2146-2157.
15. R. Jin, B. Lin, D. Li and H. Ai, *Current opinion in pharmacology*, 2014, **18C**, 18-27.
16. X. Wang, X. Xing, B. Zhang, F. Liu, Y. Cheng and D. Shi, *International journal of nanomedicine*, 2014, **9**, 1601-1615.
17. S. Dolci, V. Ierardi, A. Gradisek, Z. Jaglicic, M. Remskar, T. Apih, M. Cifelli, G. Pampaloni, C. A. Veracini and V. Domenici, *Current Physical Chemistry*, 2013, **3**, 493-500.
18. H. Gmunder, H. P. Eck and W. Droge, *European journal of biochemistry / FEBS*, 1991, **201**, 113-117.
19. Dolci S, Remskar M, Jaglicic Z, Pineider F, Boni A, Pampaloni G, Veracini CA and Domenici V, *J Mater Sci* 2013, **48**, 1283-1291.
20. M. A. Dobrovolskaia and S. E. McNeil, *Nature nanotechnology*, 2007, **2**, 469-478.
21. L. G. Delogu, E. Venturelli, R. Manetti, G. A. Pinna, C. Carru, R. Madeddu, L. Murgia, F. Sgarrella, H. Dumortier and A. Bianco, *Nanomedicine (Lond)*, 2012, **7**, 231-243.
22. M. Pescatori, D. Bedognetti, E. Venturelli, C. Menard-Moyon, C. Bernardini, E. Muresu, A. Piana, G. Maida, R. Manetti, F. Sgarrella, A. Bianco and L. G. Delogu, *Biomaterials*, 2013, **34**, 4395-4403.
23. C. Crescio, M. Orecchioni, C. Menard-Moyon, F. Sgarrella, P. Pippia, R. Manetti, A. Bianco and L. G. Delogu, *Nanoscale*, 2014, **6**, 9599-9603.
24. M. Orecchioni, D. Bedognetti, F. Sgarrella, F. M. Marincola, A. Bianco and L. G. Delogu, *Journal of translational medicine*, 2014, **12**, 138.
25. X. Chen, R. Wong, I. Khalidov, A. Y. Wang, J. Leelawattanachai, Y. Wang and M. M. Jin, *Biomaterials*, 2011, **32**, 7651-7661.
26. E. A. Vermeij, M. I. Koenders, M. B. Bennink, L. A. Crowe, L. Maurizi, J. P. Vallee, H. Hofmann, W. B. van den Berg, P. L. van Lent and F. A. van de Loo, *PloS one*, 2015, **10**, e0126687.
27. R. D. Oude Engberink, E. L. Blezer, E. I. Hoff, S. M. van der Pol, A. van der Toorn, R. M. Dijkhuizen and H. E. de Vries, *Journal of cerebral blood flow and metabolism : official journal of the International Society of Cerebral Blood Flow and Metabolism*, 2008, **28**, 841-851.
28. J. Gunn, R. K. Paranjani and M. Zhang, *Biophysical journal*, 2009, **97**, 2640-2647.
29. A. Beduneau, Z. Ma, C. B. Grotepas, A. Kabanov, B. E. Rabinow, N. Gong, R. L. Mosley, H. Dou, M. D. Boska and H. E. Gendelman, *PloS one*, 2009, **4**, e4343.
30. A. Gramoun, L. A. Crowe, L. Maurizi, W. Wirth, F. Tobalem, K. Groisdemange, G. Coullerez, F. Eckstein, M. I. Koenders, W. B. Van den Berg, H. Hofmann and J. P. Vallee, *Arthritis research & therapy*, 2014, **16**, R131.
31. A. Barrefelt, M. Saghafian, R. Kuiper, F. Ye, G. Egri, M. Klickermann, T. B. Brismar, P. Aspelin, M. Muhammed, L. Dahne and M. Hassan, *International journal of nanomedicine*, 2013, **8**, 3241-3254.
32. L. B. Thomsen, T. Linemann, K. M. Pondman, J. Lichota, K. S. Kim, R. J. Pieters, G. M. Visser and T. Moos, *ACS chemical neuroscience*, 2013, **4**, 1352-1360.
33. N. Doshi, B. Prabhakarpanidyan, A. Rea-Ramsey, K. Pant, S. Sundaram and S. Mitragotri, *Journal of controlled release : official journal of the Controlled Release Society*, 2010, **146**, 196-200.
34. T. Hyeon, S. S. Lee, J. Park, Y. Chung and H. B. Na, *Journal of the American Chemical Society*, 2001, **123**, 12798-12801.
35. D. E. Lee, H. Koo, I. C. Sun, J. H. Ryu, K. Kim and I. C. Kwon, *Chemical Society reviews*, 2012, **41**, 2656-2672.

36. C. Sciallero, D. Grishenkov, S. V. Kothapalli, L. Oddo and A. Trucco, *The Journal of the Acoustical Society of America*, 2013, **134**, 3918-3930.
37. F. Yang, L. Li, Y. Li, Z. Chen, J. Wu and N. Gu, *Physics in medicine and biology*, 2008, **53**, 6129-6141.
38. B. Xu, H. Dou, K. Tao, K. Sun, J. Ding, W. Shi, X. Guo, J. Li, D. Zhang and K. Sun, *Langmuir : the ACS journal of surfaces and colloids*, 2011, **27**, 12134-12142.
39. T. Y. Liu, H. H. Huang, Y. J. Chen and Y. J. Chen, *Acta biomaterialia*, 2011, **7**, 578-584.
40. Y. Sun, Y. Zheng, H. Ran, Y. Zhou, H. Shen, Y. Chen, H. Chen, T. M. Krupka, A. Li, P. Li, Z. Wang and Z. Wang, *Biomaterials*, 2012, **33**, 5854-5864.
41. S. T. Kang and C. K. Yeh, *Chang Gung medical journal*, 2012, **35**, 125-139.
42. S. K. Hobbs, W. L. Monsky, F. Yuan, W. G. Roberts, L. Griffith, V. P. Torchilin and R. K. Jain, *Proceedings of the National Academy of Sciences of the United States of America*, 1998, **95**, 4607-4612.
43. M. Mehrmohammadi, J. Oh, S. Mallidi and S. Y. Emelianov, *Molecular imaging*, 2011, **10**, 102-110.
44. N. Singh, G. J. Jenkins, R. Asadi and S. H. Doak, *Nano reviews*, 2010, **1**.
45. M. Mahmoudi, H. Hofmann, B. Rothen-Rutishauser and A. Petri-Fink, *Chemical reviews*, 2012, **112**, 2323-2338.
46. M. Radu, M. C. Munteanu, S. Petrache, A. I. Serban, D. Dinu, A. Hermenean, C. Sima and A. Dinischiotu, *Acta biochimica Polonica*, 2010, **57**, 355-360.
47. S. Naqvi, M. Samim, M. Abdin, F. J. Ahmed, A. Maitra, C. Prashant and A. K. Dinda, *International journal of nanomedicine*, 2010, **5**, 983-989.
48. C. H. Yeh, J. K. Hsiao, J. L. Wang and F. Sheu, *J Nanopart Res*, 2010, **12**, 151-160.
49. A. S. Arbab, G. T. Yocum, H. Kalish, E. K. Jordan, S. A. Anderson, A. Y. Khakoo, E. J. Read and J. A. Frank, *Blood*, 2004, **104**, 1217-1223.
50. G. Tosato and K. D. Jones, *Blood*, 1990, **75**, 1305-1310.
51. K. W. Moore, A. O'Garra, R. de Waal Malefyt, P. Vieira and T. R. Mosmann, *Annual review of immunology*, 1993, **11**, 165-190.
52. Y. X. Wang, *Quantitative imaging in medicine and surgery*, 2011, **1**, 35-40.
53. A. Saleh, M. Schroeter, C. Jonkmanns, H. P. Hartung, U. Modder and S. Jander, *Brain : a journal of neurology*, 2004, **127**, 1670-1677.
54. E. A. Neuwelt, P. Varallyay, A. G. Bago, L. L. Muldoon, G. Nesbit and R. Nixon, *Neuropathology and applied neurobiology*, 2004, **30**, 456-471.
55. C. von Zur Muhlen, D. von Elverfeldt, N. Bassler, I. Neudorfer, B. Steitz, A. Petri-Fink, H. Hofmann, C. Bode and K. Peter, *Atherosclerosis*, 2007, **193**, 102-111.
56. I. Siglienti, M. Bendszus, C. Kleinschnitz and G. Stoll, *Journal of neuroimmunology*, 2006, **173**, 166-173.
57. J. K. Hsiao, H. H. Chu, Y. H. Wang, C. W. Lai, P. T. Chou, S. T. Hsieh, J. L. Wang and H. M. Liu, *NMR in biomedicine*, 2008, **21**, 820-829.
58. I. Raynal, P. Prigent, S. Peyramaure, A. Najid, C. Rebutzi and C. Corot, *Investigative radiology*, 2004, **39**, 56-63.
59. A. S. Arbab, L. A. Bashaw, B. R. Miller, E. K. Jordan, B. K. Lewis, H. Kalish and J. A. Frank, *Radiology*, 2003, **229**, 838-846.

Figure Captions

Fig. 1 Cy-SPION characterization. (A) Coating around the iron-oxide nanoparticle core. (B) TEM image of the nanoparticles showing high monodispersity and average dimension of 3.95 nm. (C) Distribution of diameters through analysis of TEM images.

Fig. 2 Cy-SPION MRI properties. (A) In vitro relaxivity study at 7 Tesla of the four Cy-SPION dispersions. [Fe], relaxation rates R_1 and R_2 , Enhancement contrast ratio (EHC) are reported. (B) Image of the phantom prepared with five NMR tubes with different iron contents. Roi number 5 corresponds to water, and is used in order to highlight the contrast effect of Cy-NPs. The MRI T2-weighted image was obtained with an echo time of 100 ms and a repetition time of 2500 ms.

Fig. 3. Ultrasonography of Cy-SPION in water and whole blood.

(A) Degassed water alone (left side) or with Cy-SPION (50, 100 and 200 $\mu\text{g mL}^{-1}$) (right side) under ultrasound probe sonication in two plate wells (diameter 6.4 mm). (B) Calculation of the ultrasound signal of Fig. A (water and 200 $\mu\text{g mL}^{-1}$) (analyzed pixels= 29205). The ultrasound signal is reported in 8-bit gray scale intensity from 0 to 255 shades of gray. Signal intensity was calculated on measurements of three investigations. Degassed water was used as a negative control. *p values= 0,05. (C) Whole blood before and after injection with Cy-SPION (200 $\mu\text{g mL}^{-1}$) under ultrasonography (Scale bar 2.5mm). Red arrows highlight the particle signals. (D) Detection of Cy-SPION in a fresh whole blood filled vein phantom. A vein phantom was built specifically to assess the echogenic properties of Cy-SPION in whole blood from healthy donors. The phantom was constituted of non-toxic, non-hemolytic, and non-pyrogenic natural rubber medical tubing with no absorption/adhesion properties. Vein phantom showed a diameter of 0,5 cm. The vein phantom was filled with fresh extracted human whole blood (37 °C in heparin). As visible at the lower picture, a solution of Cy-SPION (100 μl at 200 $\mu\text{g/mL}$) was injected with a syringe; particles are clearly visible in the blood showing hyperechogenic spots (Red arrow); ultrasound images were recorded at 14.0 MHz in tissue harmonic imaging (THI) modality.

Fig. 4 Viability and proliferation assays on human primary immune cells. PBMCs were incubated with Cy-SPION at increasing doses (50 $\mu\text{g/mL}$, 100 $\mu\text{g/mL}$ and 200 $\mu\text{g/mL}$) or left untreated (medium). Data were analyzed with different stainings on flow cytometry. (A) Percentage of late apoptotic and dead cells was assessed by staining with an amine-reactive dye after 24 h of incubation; ethanol was used as a positive control. (B) Necrosis and apoptosis were assessed using propidium iodide and Annexin V staining; ethanol was used a positive control. (C) Proliferation assay was performed on stimulated cells with

phytohemagglutinin 2% (PHA) and interleukin 2 (IL2) 30 u/mL for three days. 5-ethynyl-2'-deoxyuridine (Edu) is incorporated into DNA during active DNA synthesis. Edu positive cells are reported.

Fig. 5 In silico microvasculature assay and viability under ultrasonography. (A) PBMCs were extracted from healthy donors and treated with Cy-SPION 200 µg/mL or left untreated. Cells were incubated in the synthetic microvasculature network (SMN) chip for 24 h, ultrasonography was applied for 15 minutes and viability assay (trypan blue exclusion test) was performed. (B) Phase image of a 100X zoom in the SMN with Cy-SPION treated cell; arrows indicate some of the live primary cells in the flow. (C) Viability after ultrasonography on medium control and Cy-SPION treated primary cells (Scale bar 500 µm).

Fig. 6 Activation markers analysis and cytokines secretion assay. PBMCs were treated with Cy-SPION (50, 100 and 200 µg/mL) or left untreated (medium) for 24 h. Concanavalin A (ConA, 10 µg/mL) and lipopolysaccharides (LPS 2µg/mL) were used as positive controls. (A) CD25, CD69 and CD30 cell surface activation markers were analyzed by flow cytometry. (B) Cytokine secretion was assessed by multiplex ELISA, values are expressed in pg/mL (*pvalue <0,05).

Fig. 7 Immune gene expression array. T cells were incubated with Cy-SPION (200 µg/mL) for 24 h or left untreated. The expression of 84 immune response related genes was evaluated. A) Heatmap Cy-SPION treated sample versus control medium. Genes are displayed for fold change variations versus medium control and colored by their standardized expression value (red= high expression, green= low expression) (for gene names see S. Fig. 2). B) Scatter plot. Genes upregulated with fold regulation >4 are shown in red circles. Unaffected genes are in black. C) Modulated genes versus control with a fold change >2.

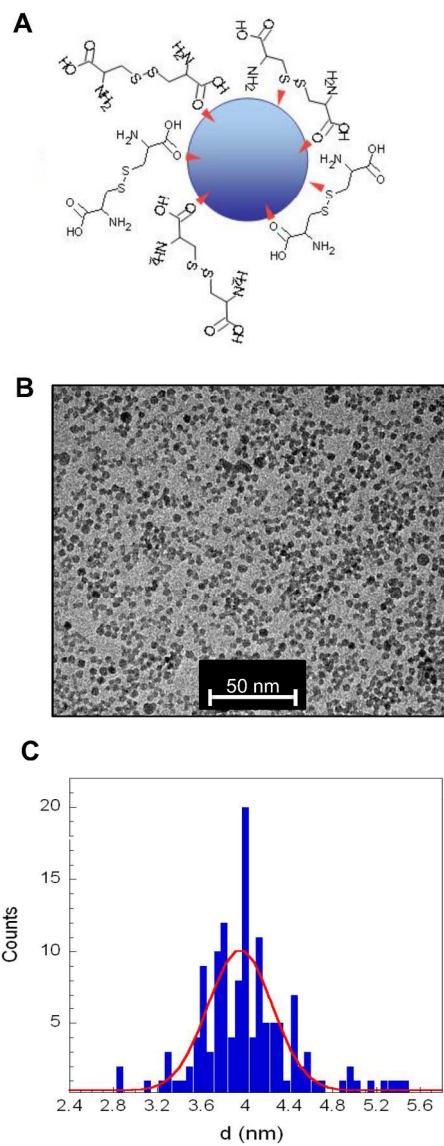


Fig. 1 Cy-SPION characterization.

219x565mm (300 x 300 DPI)

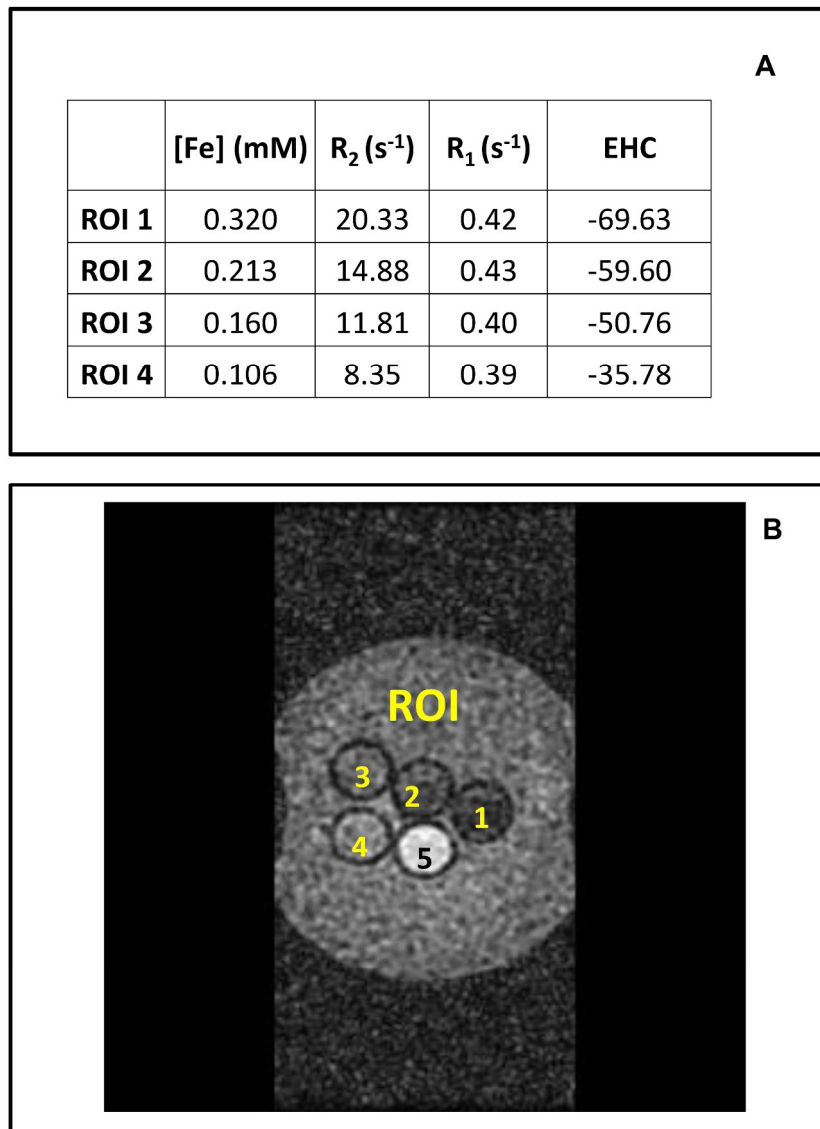


Fig. 2 Cy-SPION MRI properties

207x301mm (300 x 300 DPI)

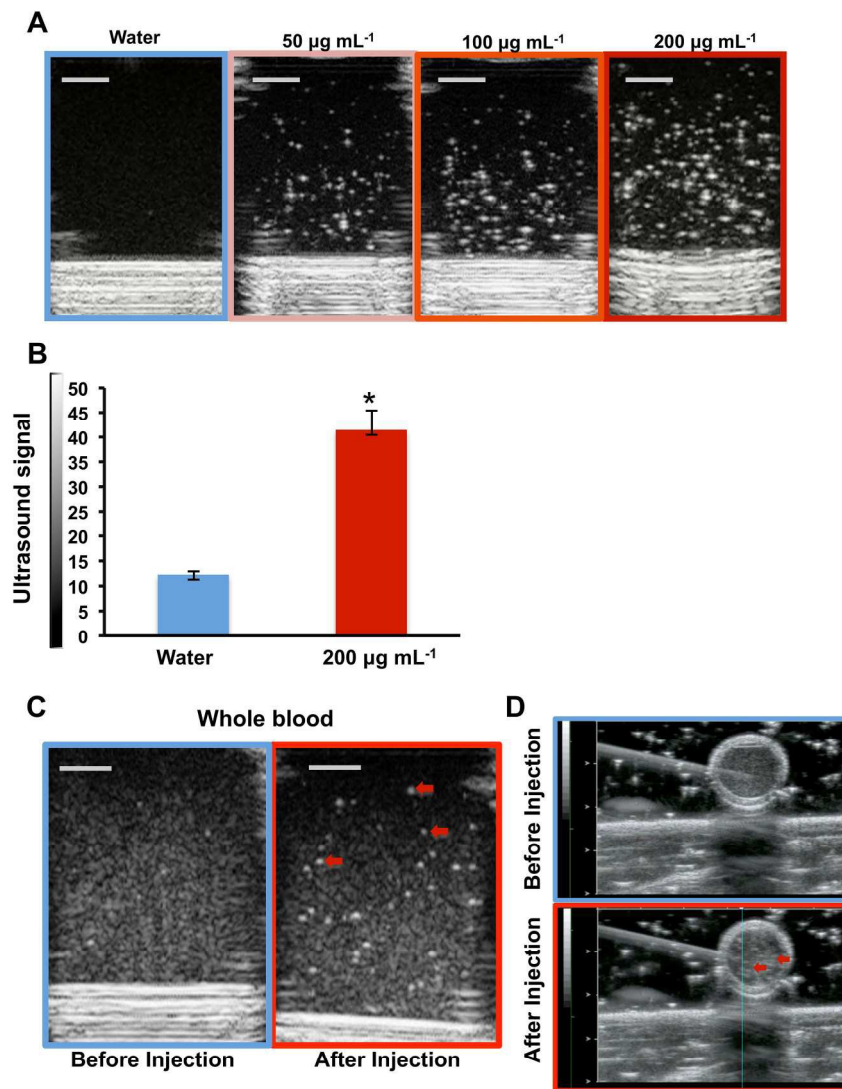


Fig. 3. Ultrasonography of Cy-SPION in water and whole blood.

199x233mm (300 x 300 DPI)

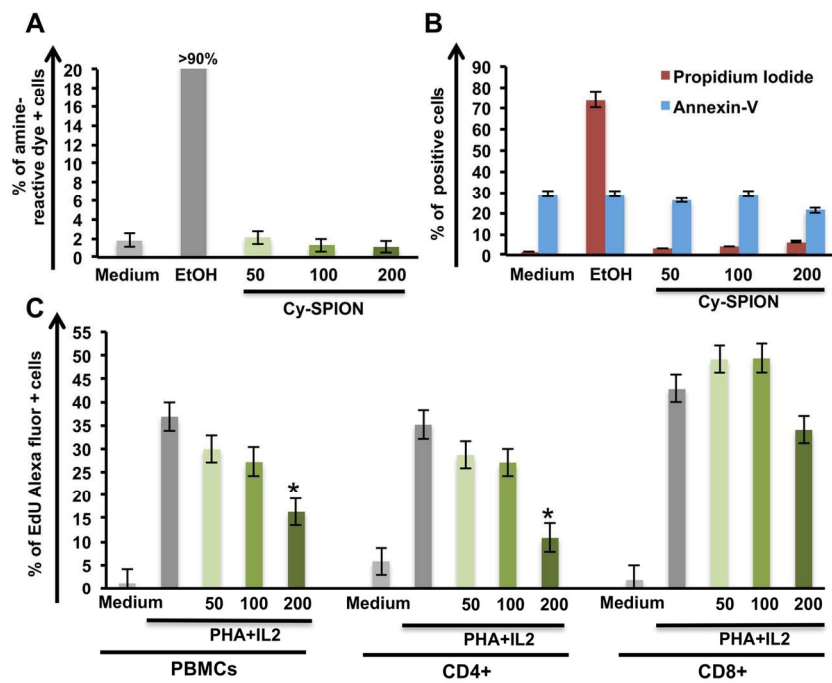


Fig. 4 Viability and proliferation assays on human primary immune cells.

145x114mm (300 x 300 DPI)

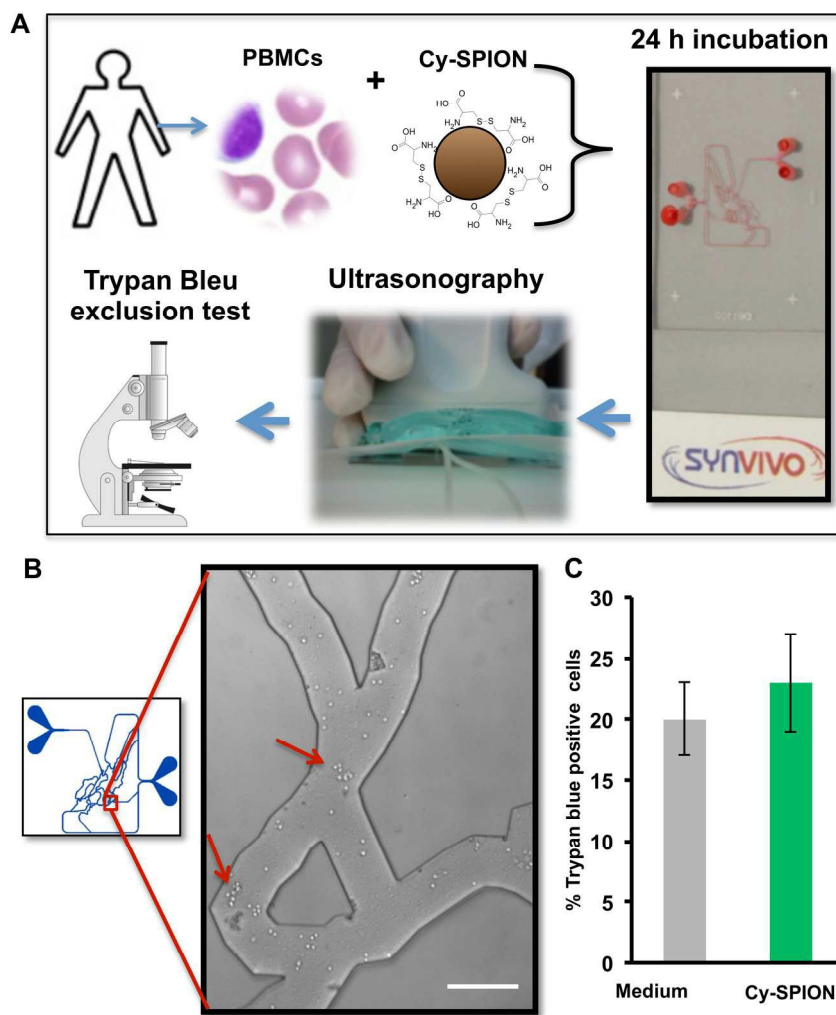


Fig. 5. In silico microvasculature assay and viability under ultrasonography.

193x205mm (300 x 300 DPI)

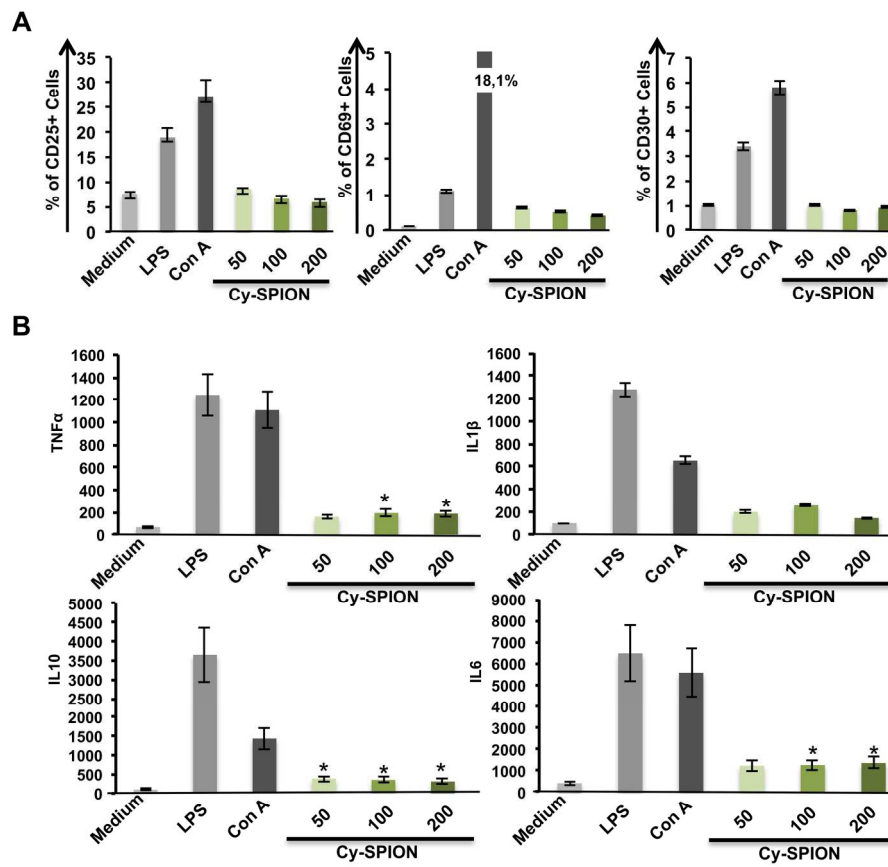


Fig. 6 Activation markers analysis and cytokines secretion assay.

184x186mm (300 x 300 DPI)

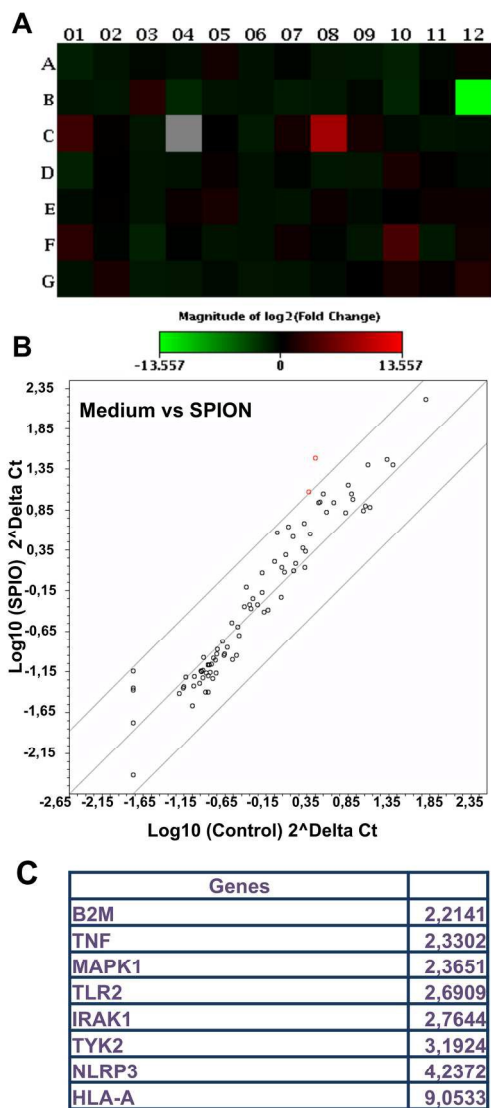


Fig. 7 Immune gene expression array.

205x242mm (300 x 300 DPI)